

COMMUNICATION

Supplement to: Selective Photocatalytic Oxidation of Benzene for the Synthesis of Phenol Using Engineered Au-Pd Alloy Nanoparticles Supported on Titanium Dioxide

Cite this: DOI: 10.1039/x0xx00000x

Received 00th January 2012,
Accepted 00th January 2012

DOI: 10.1039/x0xx00000x

www.rsc.org/

Ren Su,^a Lokesh Kesavan,^b Mads M. Jensen,^c Ramchandra Tiruvalam,^d Qian He,^d Nikolaos Dimitratos,^{b,e} Stefan Wendt,^a Marianne Glasius,^c Christopher J. Kiely,^d Graham J. Hutchings,^{b,e,*} and Flemming Besenbacher^{a,*}

Sample preparation

Colloid Preparation

Monometallic Au and Pd and three distinct Au–Pd (Au–Pd, Pd_{shell}-Au_{core}, and Au_{shell}-Pd_{core}) sols were prepared, as described below. Aqueous solutions of PdCl₂ and HAuCl₄·3H₂O (Johnson Matthey) of the desired concentration were first prepared. Fresh aqueous solutions of poly vinyl alcohol (PVA) (1 wt% aqueous solution, Aldrich, MW=10000, 80% hydrolyzed) and of 0.1 M NaBH₄ were also prepared.

(a) *Au-Pd sol*: The PdCl₂ and HAuCl₄ stock solutions were mixed in the desired ratio and the required amount (1 wt%) of a PVA solution was added ($m[\text{PVA}]/m[\text{Au} + \text{Pd}] = 1.2$); the freshly prepared solution of NaBH₄ ($n[\text{NaBH}_4]/n[\text{Au} + \text{Pd}] = 5$) was then added to the solution to form a dark-brown sol.

(b) *Pd_{shell}-Au_{core} sol*: Firstly, the required amount of a PVA solution (1 wt%) was added ($m[\text{PVA}]/m[\text{Au} + \text{Pd}] = 1.2$) to an aqueous HAuCl₄ solution of the desired concentration; a freshly prepared solution of NaBH₄ (0.1 M, $n[\text{NaBH}_4]/n[\text{Au}] = 5$) was then added to form a red sol. The solution was then stirred for 30 minutes to allow the complete reduction of all Au³⁺ in the solution. Then the required amount of the stock aqueous PdCl₂ solution was added, followed by the desired amount of NaBH₄ (0.1 M, $n[\text{NaBH}_4]/n[\text{Pd}] = 5$) to produce a dark brown sol. The solution was stirred for a further 30 minutes.

(c) *Au_{shell}-Pd_{core} sol*: The Au_{shell}-Pd_{core} sol was prepared in a similar way to that presented in (b). The required amount of PdCl₂ solution was added and reduced prior to the addition and reduction of the HAuCl₄ solution.

Colloid immobilisation

The afore-mentioned sols were immobilised onto the TiO₂ support (Degussa P25). Immobilisation of the sol was accomplished by adding TiO₂ (acidified to pH 1 by H₂SO₄) after a 30 min of sol-generation under vigorous stirring conditions. The total metal loading was maintained at 1% wt. For the random alloy series, samples having Au:Pd molar ratios of 7:1, 3:1, 1:1, 1:3 and 1:7 were prepared. After 2 h the slurry was filtered, washed thoroughly with deionized (DI) water and dried at 120 °C for 16 h.

Details of the preparation procedures are also available from our previous work.¹

Photocatalyst characterisations

TEM/STEM

The as-prepared sol-immobilised catalysts were prepared for TEM/STEM analysis by dry dispersing the catalyst powder onto a holey carbon TEM grid. HRTEM and HAADF imaging was carried out using a 200kV JEOL 2200FS TEM equipped with a CEOS probe aberration corrector. Figure S1 shows the representative HRTEM images of the Au₁Pd₁ and Pd_{shell}-Au_{core} NPs supported on TiO₂ and the derived particle size distributions of the metal NPs. Details of the analysis can be found in some of our previous publications.¹⁻³

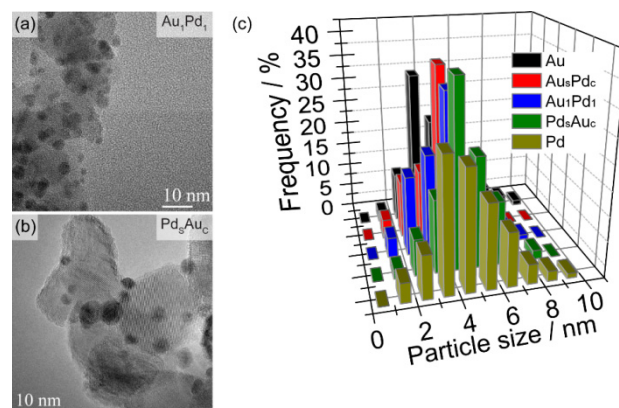


Figure S1. (a) Representative low magnification HRTEM images of as-prepared (a) Au₁Pd₁ and (b) Pd_{shell}-Au_{core} NPs supported on TiO₂. (c) Particle size distributions of the NPs derived from HRTEM images.³

XRD & BET

Crystallographic information relating to the TiO₂ support material after sol-immobilisation was acquired *via* X-ray diffractometry (SmartLab, Rigaku employing Cu-K_α radiation). The metal decoration did not change the crystallographic polymorph distribution of the TiO₂ support (Fig. S2a), and the TiO₂ polymorph composition was identical for all samples (Fig. S2b). The metal loading and particle size was too low to be

detected by XRD. The N₂ adsorption analysis (Figs. S2c and S2d) of selected samples shows they have very similar surface areas and are very close, within experimental error, to that of the pure TiO₂ support ($\sim 50 \text{ m}^2 \cdot \text{g}^{-1}$).³

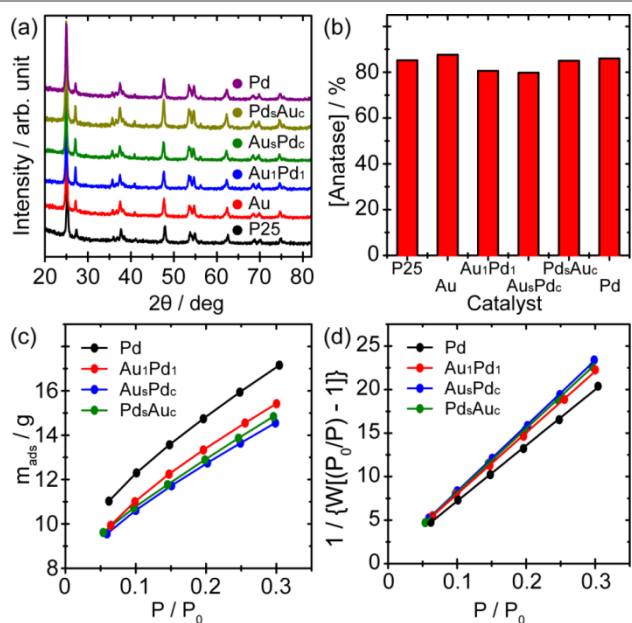


Figure S2. (a) XRD patterns of Au, Au_{shell}-Pd_{core}, Au₁Pd₁, Pd_{shell}-Au_{core}, and Pd NPs supported on TiO₂; XRD from a pristine TiO₂ support (P25) is also presented for comparison. (b) Derived polymorph composition of the TiO₂. (c) N₂ adsorption isotherms and (d) BET plots from selected catalyst samples. The derived surface areas are 53.7, 48.7, 45.8, and 46.8 m²·g⁻¹ for Pd/TiO₂, Au₁Pd₁/TiO₂, Au_{shell}-Pd_{core}/TiO₂, and Pd_{shell}-Au_{core}/TiO₂, respectively.³

Methodology for photocatalytic tests

Optical property of the samples

The light responses of the samples are summarized in Fig. S3(a) by means of diffuse reflectance spectroscopy (DRS). Only the Au/TiO₂ sample showed a considerable reduction of the reflectance in the 450 – 650 nm wavelength range compared to the rest of the samples (Fig. 2a), which originated from the Au surface plasmon. The spectra indicate that no visible light absorption ($\lambda > 400 \text{ nm}$) was observed any other samples except Au/TiO₂.

Light source

A UV LED (365 nm, Optimax 365) light source was used in all photocatalysis experiments. The light source has a peak emission at 365 nm with a full-width-at-half-maximum (FWHM) of 10 nm, as shown in Fig. S3(b). This eliminated the possibility of visible light photoreactivity of the Au/TiO₂ sample (if any) and allowed for direct comparison with the other samples.

The average photon flux of the light source was measured using a standard ferrioxalate actinometry method and was found to be $\sim 4 \times 10^{17} \text{ photons} \cdot \text{s}^{-1}$.³

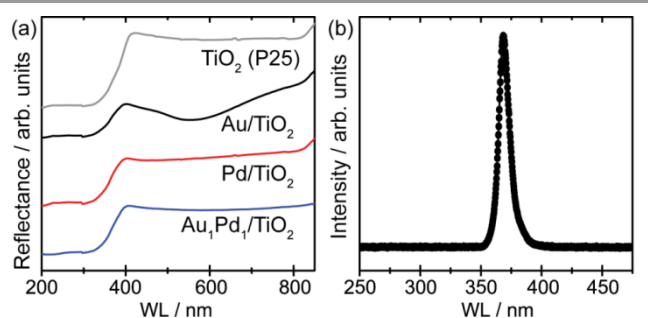


Figure S3. (a): Diffuse reflectance spectra of pure TiO₂, Au/TiO₂, Pd/TiO₂, and Au₁Pd₁/TiO₂ samples. The spectra have been offset arbitrarily for better visibility. (b): the emission spectrum of the light source used for all experiments.

Apparatus and protocols for photocatalytic benzene oxidation

Photo-oxidation of benzene was carried out under aerated conditions at room temperature. A leak-tight reactor that was designed for *in-situ* UV-vis spectrometry analysis is shown in Fig. S4. The cuvette and the viewport were made of quartz. The total volume of the reactor was 125 mL. Magnetic stirring was applied throughout the reaction, and we have confirmed that the equilibrium of the diffusion can be achieved within 30 s under our stirring conditions. A 100 mg·L⁻¹ photocatalyst-water suspension was prepared, sonicated for 1 min, and UV cleaned for 2 h under continuous stirring to remove the capping ligands. Then the concentrated suspension was diluted 20 times (catalyst loading of 5 mg·L⁻¹) and transferred into the reactor to prepare a 100 mL of diluted suspension for photocatalytic reactions. The reactor was then mounted to the UV-vis spectrometer with continuous stirring (see Fig. S4). A series of UV-vis spectra were sequentially recorded for 1 h with a time interval of 5 min. A stable background was achieved after $\sim 30 \text{ min}$, indicating the equilibrium state of the suspension. A 8.9 μL of benzene ($\geq 99\%$, Sigma Aldrich) was subsequently added into the suspension to form the 1 mM benzene-catalyst suspension. Then all valves were closed to prevent the evaporation of benzene. The UV-vis spectra were continuously recorded for another 30 min with a time interval of 5 min until the benzene peaks stabilised. The UV irradiation was then commenced and UV-vis spectra were recorded *in-situ* at regular time intervals for all samples, as shown in Fig. S5.

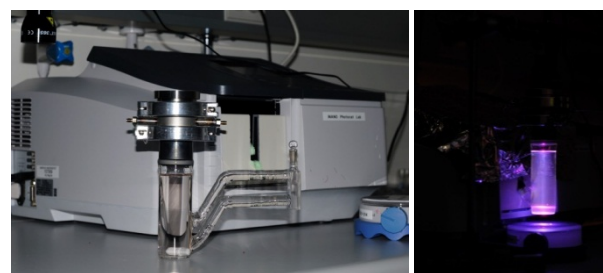


Figure S4. Apparatus for recording UV-vis spectra time sequences during benzene oxidation with our photocatalysts.

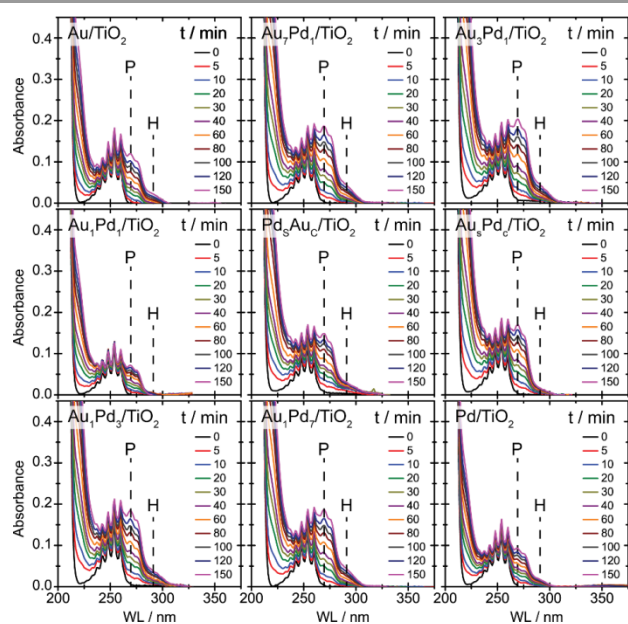


Figure S5. *In situ* UV-vis spectra time sequences recorded during benzene oxidation for all photocatalysts in this study. P and H denote phenol and hydroquinone, respectively.

Liquid phase products analysis

The absorption spectra of phenolic compounds along with benzene are shown in Fig. S6(a). A characteristic sextet of absorption peaks for benzene are located at ~ 250 nm with absorption coefficients (ϵ) of 19 (233 nm), 48 (243 nm), 76 (248 nm), 90 (254 nm), and 64 (260 nm) $M^{-1}cm^{-1}$, respectively (Fig. S6b). The light absorption of benzene at $\lambda > 270$ nm was found to be negligible. The absorption peaks of phenol, hydroquinone, and catechol are located at 270, 289, and 275 nm, respectively, and all ϵ values were orders of magnitude higher than that of benzene, as shown in Fig. S6(c)–(e) and listed in Table S1.⁴ Note that the absorption peak of benzoquinone ($\lambda_{max} = 246$ nm) overlaps with that of benzene; however, it should be relatively easy to observe the evolution of benzoquinone (if any is generated) due to its extremely large ϵ value (16649 $M^{-1}cm^{-1}$) and distinct peak shape compared to that of benzene. Therefore, in our *in-situ* UV-vis experiments, the formation of benzoquinone was determined to be negligible and the concentrations of the phenolic products can be estimated using the following equations that have been reported in our previous work.⁴

$$A_{289} = \epsilon_H^{289} \times C_H + \epsilon_C^{289} \times C_C + \epsilon_P^{289} \times C_P \quad (1)$$

$$A_{275} = \epsilon_H^{275} \times C_H + \epsilon_C^{275} \times C_C + \epsilon_P^{275} \times C_P \quad (2)$$

$$A_{270} = \epsilon_H^{270} \times C_H + \epsilon_C^{270} \times C_C + \epsilon_P^{270} \times C_P \quad (3)$$

where

ϵ is the absorption coefficient;

C is the concentration;

Subscripts H, C, and P denote hydroquinone, catechol, and phenol, respectively. The absorption coefficients were listed in Table S1.

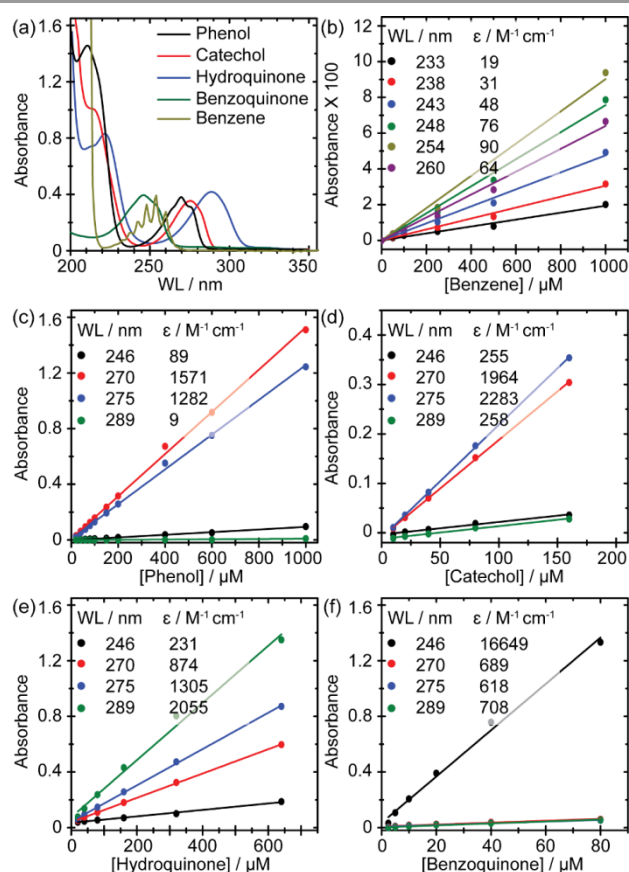


Figure S6. (a) Absorption spectra of phenolic compounds and benzene. (b)–(f) Absorption coefficients of benzene and the phenolic compounds at a series of specific wavelengths determined using various concentrations.

Table S1. Absorption coefficients of phenol, hydroquinone, catechol, and benzoquinone at a series of specific wavelengths.

Products	Coefficient / $M^{-1}cm^{-1}$			
	246 nm	270 nm	275 nm	289 nm
Phenol	89	1571	1282	9
Benzoquinone	16649	689	618	708
Catechol	255	1964	2283	258
Hydroquinone	231	874	1305	2055

Ultra high performance liquid chromatography coupled by an electrospray ionisation inlet to a quadrupole time-of-flight mass spectrometer (UHPLC-ESI-QTOF-MS, Dionex Ultimate 3000 UHPLC+ coupled to Bruker microOTOF-Q) was utilised to determine any other possible liquid phase byproducts (*i.e.*, polycarboxylic acids).

The liquid samples for UHPLC-ESI-QTOF-MS were prepared using the following procedure:

First, a 100 $mg \cdot L^{-1}$ photocatalyst-water suspension was prepared using the $Au_{shell}Pd_{core}/TiO_2$ sample, sonicated for 1 min, and UV cleaned for 2 h under continuous stirring to remove the capping ligands. Then 8.9 μL of benzene ($\geq 99\%$, Sigma Aldrich) was added into the suspension to form the 1 mM benzene-catalyst suspension. Subsequently, the suspension was continuously stirred in dark conditions for 30 min to reach adsorption equilibrium. The reactor was sealed to prevent the evaporation of benzene. UV irradiation was then commenced

and 3 mL of aliquots were taken at given time intervals (0, 10, 20, 30, and 60 min) and immediately centrifuged to remove the photocatalysts. Finally, the clear liquid samples were filtered through syringe filters (0.22 μm pore size Q-Max PTFE/L) prior to analysis.

The following parameters were used for UHPLC analysis. A Waters ACQUITY UPLC HSS T3 column was kept at 45 $^{\circ}\text{C}$ during the analysis (particle size 1.8 μm , C_{18} phase, 100 x 2.1 mm), and the sample injection volume was 20 μL . Eluents A and B were 0.1% acetic acid and 0.1% acetic acid in acetonitrile, respectively, and the flow rate was 0.3 mL min^{-1} . The applied 17 min eluent gradient was eluent B kept at 3% for 1 min, increased to 25% in 9 min, increased to 95% in 2.5 min and kept at 95% for 2.5 min before returning to 3% B. The analysis of carboxylic acids was achieved by MS detection in negative ESI mode in a m/z range of 50-1000 using a modified method described by Kristensen and Glasius.⁵ Positive ESI mode revealed neither significant peaks nor differences between samples (data not shown).

Extracted ion chromatograms (EICs) of significant peaks from negative ESI mode are shown in Fig. S7. Table S2 lists all possible by-products. It was clear that the most intense peak was identified as catechol, which has been determined to be less than 6 μM after UV irradiation of 60 min by UV-vis spectrometry. Since all the rest of the peaks were much less intense than that of catechol, it indicates the concentrations of these compounds should be far less than 6 μM based on the assumption that they have similar relative sensitivity factors.

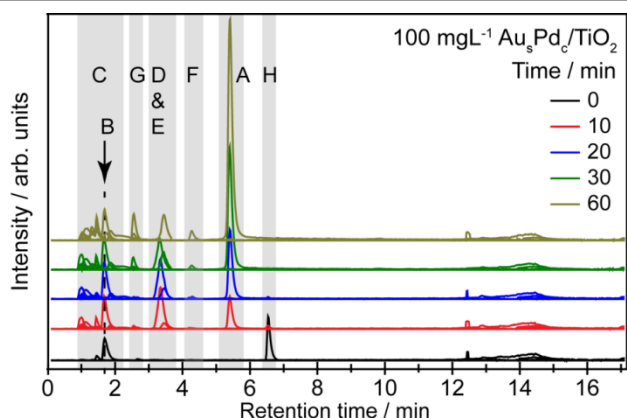


Figure S7. Extracted ion chromatograms (EICs) from negative mode LC-MS of liquid phase samples from photocatalytic benzene oxidation at different irradiation time. $\text{Au}_{\text{shell}}\text{Pd}_{\text{core}}/\text{TiO}_2$ was used as the photocatalyst with a loading of 100 mg L^{-1} . Legends denotation: A: Catechol, B: succinic acid, C: short-chain carboxylic acids, D: hydroxyhydroquinone, E: hydroxybenzoquinone, F: resorcinol, G: unknown (m/z : 492.06), likely to be a benzenediol polymer, H: unknown (m/z : 172.10). The spectra were stacked without scaling for better visualization, and the maximum peak intensity was 1×10^5 (catechol).

We also observed small but distinct peaks with masses corresponding to C_3 - C_4 hydroxycarboxylic acids, C_3 - C_5 ketocarboxylic acids, C_4 unsaturated dicarboxylic acids and C_3 - C_4 saturated dicarboxylic acids with retention times of 0.9-2.5 min by using EICs of the respective ion $m/z \pm 0.005$. The succinic acid peak at 1.6 min is shown as B in Fig. S7. The low signal intensity of the carboxylic acids did not facilitate identification by MS^2 fragmentation. Tentative quantification using malonic acid suggests that the concentration of each carboxylic acid is less than 10 μM .

Table S2. Possible liquid phase byproducts determined by UHPLC-ESI-QTOF-MS

ID	m/z	Compound	Concentration
A	109.03	catechol	< 6 μM (a)
B	117.02	succinic acid	<< 10 μM (b)
C	N/A	carboxylic acids	<< 10 μM (b)
D	123.01	hydroxy-benzoquinone	<< 6 μM (c)
E	125.02	hydroxy-hydroquinone	<< 6 μM (c)
F	109.03	resorcinol (d)	<< 6 μM (c)
G	492.06	unknown (e)	<< 6 μM (c)
H	172.10	unknown (f)	<< 6 μM (c)

(a): The concentration determined by UV-vis.

(b): Quantified by malonic acid reference.

(c): Based on the assumption that these molecules have similar relative sensitivity factor.

(d): Expected to be resorcinol due to the identical mass to catechol.

(e): Expected to be benzenediol polymer.

(f): Only observed in the liquid sample before irradiation.

Gas phase product analysis

The CO_2 evolution from the complete oxidation of benzene and phenol was carried out in a leak-tight reactor that was connected to a mass spectrometer (MS, Hiden HPR-20). The same amount of photocatalyst that was used in the *in-situ* UV-vis reactor was dispersed in 25 ml of 1 mM benzene/phenol solution and kept in the dark for 30 min to establish adsorption equilibrium prior to experiment. A 5.5 hour irradiation was employed for the CO_2 evolution process under continuous stirring and the partial pressures of $m/e^- = 18$ (H_2O), 28 (N_2), 32 (O_2), and 44 (CO_2) were monitored *in-situ*. Deionised (DI) water and the same UV LED light was used throughout the experiments. Details of the photo-reactivity measurements and related calculations have been reported in detail in our previous work.^{3,4}

High loading test & evaluation of quantum efficiency

We have discussed the effect of metal co-catalyst using a low catalyst loading, which avoided the excessive scattering of light that originated from the TiO_2 NPs during the *in-situ* UV-vis measurements. The advantages of *in-situ* UV-vis analysis are obvious; however, one downside is that the light cannot be fully absorbed by the photocatalysts due to their low concentration. In order to evaluate the performance under a more realistic conditions, we performed benzene oxidation using the best photocatalyst, $\text{Au}_{\text{shell}}\text{Pd}_{\text{core}}/\text{TiO}_2$ at a much higher loading of 100 mg L^{-1} (20 times higher than the low loading test). Note that at such high photocatalyst loading, *in-situ* UV-vis spectrometry method cannot be used due to the strong scattering by the TiO_2 NPs. Therefore, we have to use *ex-situ* UV-vis spectrometry instead. In this case, 2 mL of aliquots were withdrawn at given time intervals, centrifuged for 10 min and measured immediately by UV-vis, as shown in Fig. S8(a). Evolution of the phenolic products that were derived from the UV-vis spectra is shown in Fig. S8(b). It is clear that the

production of phenol was significantly enhanced (~ 7 times) compared to that of at low catalyst loading case, as $\sim 140 \mu\text{M}$ of phenol have been produced within 30 min of irradiation. We also observed the evolution of benzoquinone (B) instead of hydroquinone (H) during the *ex-situ* UV-vis measurement, which was evolved from the oxidation of hydroquinone during the time elapsed before *ex-situ* UV-vis measurements.

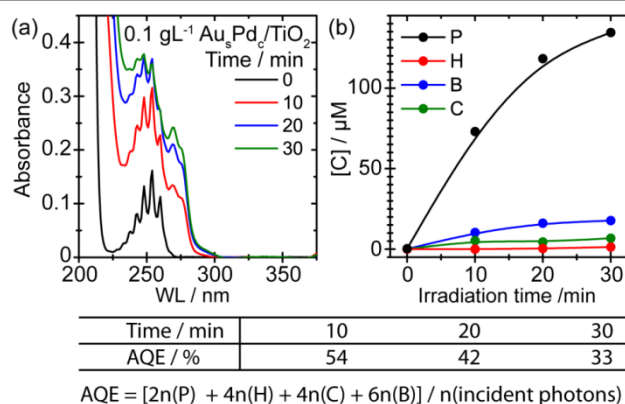


Figure S8. (a) *Ex-situ* UV-vis spectra time sequences recorded for benzene oxidation using the $\text{Au}_{\text{shell}}\text{Pd}_{\text{core}}/\text{TiO}_2$ NPs supported on TiO_2 with a catalyst loading of 0.1 gL^{-1} . (b) Evolution of phenol (P), hydroquinone (H), benzoquinone (B), and catechol (C) derived from the UV-vis spectra. The calculated apparent quantum efficiencies (AQE) are given below the figures.

We have also estimated the apparent quantum efficiency (AQE) for the generation of phenolic products at different times. Clearly, the $\text{Au}_{\text{shell}}\text{Pd}_{\text{core}}/\text{TiO}_2$ photocatalyst showed decent AQEs within the irradiation period. A drop of AQE was observed after prolonged irradiation time, which may arise from the complete oxidation of benzene and the produced phenolic compounds.

Notes and references

^a Interdisciplinary Nanoscience Center (iNANO) and Department of Physics and Astronomy, Aarhus University, DK-8000 Aarhus C, Denmark.

^b Cardiff Catalysis Institute, School of Chemistry, Cardiff University, Cardiff, CF10 3AT, UK.

^c Department of Chemistry and Interdisciplinary Nanoscience Center (iNANO), Aarhus University, Langelandsgade 140, DK-8000 Aarhus C, Denmark.

^d Department of Materials Science and Engineering, Lehigh University, 5 East Packer Avenue, 18015-3195, Bethlehem, Pennsylvania, USA.

^e The UK Catalysis Hub, Research Complex at Harwell, Rutherford Appleton Laboratory, Oxfordshire, OX11 0FA, UK.

† The authors acknowledge the CMC (Denmark National Research Foundation, DNRF 93), the Danish Strategic Research Council, the Carlsberg Foundation, an advanced grant for ERC (FB) and the EPSRC, and NSF for financial support.

1. J. Pritchard, L. Kesavan, M. Piccinini, Q. He, R. Tiruvalam, N. Dimitratos, J. A. Lopez-Sanchez, A. F. Carley, J. K. Edwards, C. J. Kiely and G. J. Hutchings, *Langmuir*, 2010, **26**, 16568.

2. R. C. Tiruvalam, J. C. Pritchard, N. Dimitratos, J. A. Lopez-Sanchez, J. K. Edwards, A. F. Carley, G. J. Hutchings and C. J. Kiely, *Faraday Discuss.*, 2011, **152**, 63.

- R. Su, R. Tiruvalam, A. J. Logsdail, Q. He, C. A. Downing, M. T. Jensen, N. Dimitratos, L. Kesavan, P. P. Wells, R. Bechstein, H. H. Jensen, S. Wendt, C. R. A. Catlow, C. J. Kiely, G. J. Hutchings and F. Besenbacher, *ACS Nano*, 2014, **8**, 3490.
- R. Su, R. Tiruvalam, Q. He, N. Dimitratos, L. Kesavan, C. Hammond, J. A. Lopez-Sanchez, R. Bechstein, C. J. Kiely, G. J. Hutchings and F. Besenbacher, *ACS Nano*, 2012, **6**, 6284.
- K. Kristensen and M. Glasius, *Atmos. Environ.*, 2011, **45**, 4546.